Journal of Hydrology 587 (2020) 124869

Contents lists available at ScienceDirect

Journal of Hydrology

journal homepage: www.elsevier.com/locate/jhydrol

Research papers

Combined effects of urbanization and climate change on watershed evapotranspiration at multiple spatial scales

Di Fang[a,b], Lu Hao[a,*], Zhen Cao[a], Xiaolin Huang[a], Mengsheng Qin[a], Jichao Hu[c,a], Yongqiang Liu[d], Ge Sun[e]

[a] Jiangsu Key Laboratory of Agricultural Meteorology, Nanjing University of Information Science and Technology, Nanjing 210044, China
[b] Guizhou Institute of Mountain Environment and Climate, Guiyang 550002, China
[c] China Meteorological Administration (CMA)/Henan Key Laboratory of Agrometeorological Support and Applied Technology, Zhengzhou 450003, China
[d] Center for Forest Disturbance Science, Southern Research Station, USDA Forest Service, Athens, GA 30602, USA
[e] Eastern Forest Environmental Threat Assessment Center, Southern Research Station, USDA Forest Service, Research Triangle Park, NC 27709, USA

ARTICLE INFO

Keywords:
Urbanization-associated land cover change
Climate warming
SWAT model
Ecohydrological processes
Rice paddy watershed

ABSTRACT

How urbanization-associated land use/land cover change (LULCC) affects the ecohydrological cycle through altering evapotranspiration (ET) processes is not clear for rice paddy dominated watersheds. The purpose of this study was to understand long-term (2000–2013) spatial and temporal variations of ET over the Qinhuai River Basin in a humid region, southern China. We revised the Soil and Water Assessment Tool (SWAT) by incorporating new algorithms describing hydrological processes of rice paddies. Using the improved SWAT model driven by remote sensing-derived LULCC and local climatic data, we separated the effects of LULCC on ET from climate at the watershed scale. We showed that the modified SWAT model significantly improved monthly streamflow estimates. The Nash-Sutcliffe model efficiency (*NSE*) was 0.86 and coefficient of determination (R^2) was 0.88 for the calibration period (1990–1994) while the *NSE* was 0.65 and R^2 was 0.71 for the validation period (1995–1999). We also found good agreements between modelled daily ET and lysimeter-based measurements for an experimental rice paddy field (R^2 = 0.75, p less than 0.01). For areas with little land cover change, ET rates increased over time due to the increase in potential ET (PET) during 2000–2013. However, the contribution from rice paddy to the watershed-level ET decreased over time coincident with a period of rapid urbanization and loss of rice paddy field. Dynamic attribution analysis indicated that the negative contribution of LULCC to change in ET increased from 53% in 2000 to 61% in 2013 while the positive contribution of climate variability decreased from 47% in 2000 to 39% in 2013. We concluded that factors affecting ET varied with spatial scale. Conversion of rice paddy field to urban use directly resulted in significant ET reduction at the watershed scale despite the rise in the air temperature and potential ET in the study region. The improved SWAT model provides a better integrated method for understanding ET processes and assessing the impacts of environmental change on ecosystem services in a rapidly urbanizing region.

1. Introduction

Urbanization and associated land use and land cover change (LULCC) has been widely recognized to have negative influences on ecosystems by altering watershed hydrology (Paul and Meyer, 2011; Sun and Lockaby, 2012). LULCC and associated anthropogenic activities cause losses of ecosystem functions (Fan et al., 2016) through altering flood frequency (Brath et al., 2006; Crooks and Davies, 2001; Gao and Sang, 2017) and seasonal streamflow patterns (Guo et al., 2008), impairing water quality (Sun and Lockaby, 2012), and aggravating Urban Heat Island (Hao et al., 2015a; Zhao et al., 2014) and Urban Dry Island (Hao et al., 2018). Climate change is also becoming a major threat to natural resources such as water supply and crop production in many parts of the world (Piao et al., 2010; Kim et al., 2015; Cao et al., 2011; Martin et al., 2017; Zhao et al., 2019a,b). For example, the average air temperature in China has increased (Gao et al., 2002), and precipitation significantly increased in southern China affecting regional evaporation and transpiration rates (Merritt et al., 2006). However, the regional hydrologic impacts of climate variability may be completely different those from LULCC due to the contrasting underlying physical and biological processes (Martin et al., 2017; Sun et al., 2019; Zhao et al., 2020a,b). Separating the individual effects of climate

* Corresponding author.
E-mail address: haolu@nuist.edu.cn (L. Hao).

https://doi.org/10.1016/j.jhydrol.2020.124869

Available online 24 March 2020

change and land-use/land-cover change is not only essential for interpreting ecohydrological change and its drivers (Eum et al., 2016), but also for watershed management decision making.

Rice paddy field, a major land-use for agricultural food production in southern China, provides similar ecosystem service benefits like other wetlands, such as water quality improvement (Kang et al., 2006) and climate moderation (Hao et al. 2015a; Hao et al., 2018). However, growing rice consumes a large amount of water due to its irrigation needs. Thus, converting rice paddy to urban uses in the process of urbanization is projected to have profound impacts on the watershed hydrological cycle (Hao et al., 2015a). Our previous study (Hao et al., 2015a) found that urbanization and climate warming (Qin et al., 2019) in a rapidly urbanizing rice paddy-dominated watershed in eastern China collectively elevated streamflow by 58% due to a decrease in ET by 23% during 1986–2013. However, we know little about the effects of individual and combined changes in LULCC and climate change on watershed hydrological processes due to the complexity of rice paddy management in watersheds with mixed land uses amid climate change (Hao et al., 2015a).

Hydrological response to disturbances is scale dependent. A watershed modelling study in a rice paddy-dominated region in southern China suggests that converting rice paddies to urban area reduces overall water consumption (Tsai, 2002). The hydrological processes of rice paddy-dominated watersheds are extremely complex due to the mixed compositions of LULCC. For example, Xu et al. (2017) found that simulated ET by the traditional Penman-Monteith model for rice paddy overestimated or underestimated ET because of large daily variations in net radiation, soil heat flux and soil moisture in Kunshan region of China. The dominated controlling factors for ET vary across spatial scales (Mauser and Schädlich, 1998; Xu and Yang, 2010; Cristiano et al., 2015; Zhang et al., 2016). Amatya et al. (2014) suggest that soil, plant type, and regional weather conditions, are important for explaining ET response to land management at a landscape scale while ET is dominated by climatic conditions at a regional scale. Similarly, Zhou et al. (2013) concludes that ET is controlled by water availability at a plot scale but is sensitive to energy available as well as surface temperature at a regional scale.

Process-based simulation models are useful tools to quantify the influence of climate (e.g. precipitation, relative humidity, temperature and radiation) and human activities (e.g., irrigation, urbanization, and drainage operations) on watershed hydrology (Xie and Cui, 2011; Du et al., 2012; Hao et al., 2015b). Among many existing hydrological models, the Soil Water Assessment Tool (SWAT) has been widely used because of its versatility and open sources (Sun et al., 2017; Zhao et al., 2019a,b; Wu et al., 2016). SWAT as a process-based watershed model describes the essential hydrological processes and is capable for assessing the impacts of agricultural practices on water quality, providing an effective tool for environmental assessment and watershed management (Fan et al., 2016; Laurent and Ruelland, 2011). However, SWAT has not been applied widely in modelling hydrological processes in rice paddy-dominated watersheds. Previous modification of the SWAT model simply treats rice field as a pothole or an impoundment. The original pothole module in SWAT assumes that the water surface evaporation is actual ET in rice field. Sakaguchi et al. (2014) developed a modified paddy module in SWAT and modelled the hydrological processes in a 3-km^2 paddy field. Xie and Cui (2011) incorporated a new irrigation scheme to SWAT for simulating streamflow in Zhanghe Irrigation District of southern China. Kang et al. (2006) incorporated the total maximum daily load system within the SWAT model to evaluate water balance and water quality in irrigated rice paddy region in South Korea. However, these studies rarely examined model performance in modelling ET, a major hydrological component in a humid region and one of the most uncertain hydrologic variables that plays a key role in determining watershed water balance, assessing effects of LULCC on local and climate, scheduling agricultural irrigation (Aouissi et al., 2016; Abdullah et al., 2014; Chirouze et al., 2014; Qiu et al., 2015; Liu et al., 2017a), and assessing climate change impacts (Falamarzi et al., 2014; Shiri et al., 2012, Wang and Liang, 2008).

We chose the Qinhuai River Basin (QRB) for this case study to understand hydrological response, ET in particular, to urbanization and climate change at spatial multiple scales. The QRB represents a typical watershed on the Yangtze River Delta (YRD), one of the most developed and highly populated regions in China (Hao et al., 2018). The region is facing serious environmental challenges such as flood risk and water quality deterioration (Zhou et al., 2013), local climate change such as Urban Heat Islands (UHIs) (Hao et al., 2015a) and Urban Dry Islands (UDI) (Hao et al., 2018) and global warming (Gu et al., 2011). Understanding the impacts of climate change and LULCC on watershed hydrology is essential to mitigating global climate change and local LULCC, and most importantly offering scientific principles to guide watershed ecosystem restoration efforts (Zhou et al., 2013; Chien et al., 2013).

We hypothesized that the dominated driving factors for ET change varied across spatial scales, and LULCC was the main cause of ET reduction in the study basin. The overall goal of this modelling study was to understand the individual and combined impacts of LULCC and climate change on ecohydrological processes, ET in particular. The specific objectives were: (1) to modify, calibrate, and validate an improved SWAT model for estimating ET at different temporal and spatial scales, (2) to examine the response of ET to disturbance by land-cover type, and (3) to quantify the individual contributions of climate and LULCC to ET variations over a 14-year period at a watershed scale.

2. Materials and methods

2.1. Study area

The QRB, one of the tributaries of the Yangtze River, covers most of the administrative area of Nanjing City, the capital of Jiangsu Province (118.39 − 119.21° E longitudes and 31.30 − 32.10° N latitudes) (Fig. 1). As a highly human-impacted watershed, the QRB has two main flow outlets, Wuding and Inner Qinhuai Sluice Gates. Flat topography characterizes most part of the watershed except the northeast. The basin has an area of approximately 2,631 km^2 with an elevation ranging from 0 to 410 m. The study region is dominated by the East Asia summer monsoon climate (Gu et al., 2011), with an average annual temperature and total precipitation of 15.4 °C and 1116 mm, respectively. The QRB has experienced global warming with mean air temperature increased at a rate of 0.44 °C per decade, and thus an increasing evaporative potential during the past two decades (Hao et al., 2015a). Nearly 75% of the annual precipitation falls during April to October as the rainy season. The dominant land cover type in this watershed is rice paddy (RICE), followed by urban area (URHD), water body (WATR), forests (FRST) and dry agricultural land (AGRC). The QRB has experienced a rapid urbanization since 2002 (Hao et al., 2015a) at the expense of rice paddies and other land types (Du et al., 2013). During the past decade, the area of rice paddies has significantly reduced by 7.6%, followed by agricultural land (2.4%), water body (0.6%), and forests (0.5%), in contrast to the notable increase in urban area of 11.3%.

2.2. SWAT model

The SWAT model was selected in this study for assessing the hydrological impacts of LULCC and climate change and variability on watershed (QRB) ET for three different periods (2000–2003, 2004–2008, 2009–2013). Our previous empirical studies indicated that the QRB had been significantly impacted by urbanization and climate change in both hydrology (i.e., streamflow and ET) and local meteorology (Hao et al., 2015a; Qin et al., 2019; Hao et al., 2018).

The SWAT model is a semi-distributed continuous hydrologic model operated in a Geographic Information System (GIS) environment

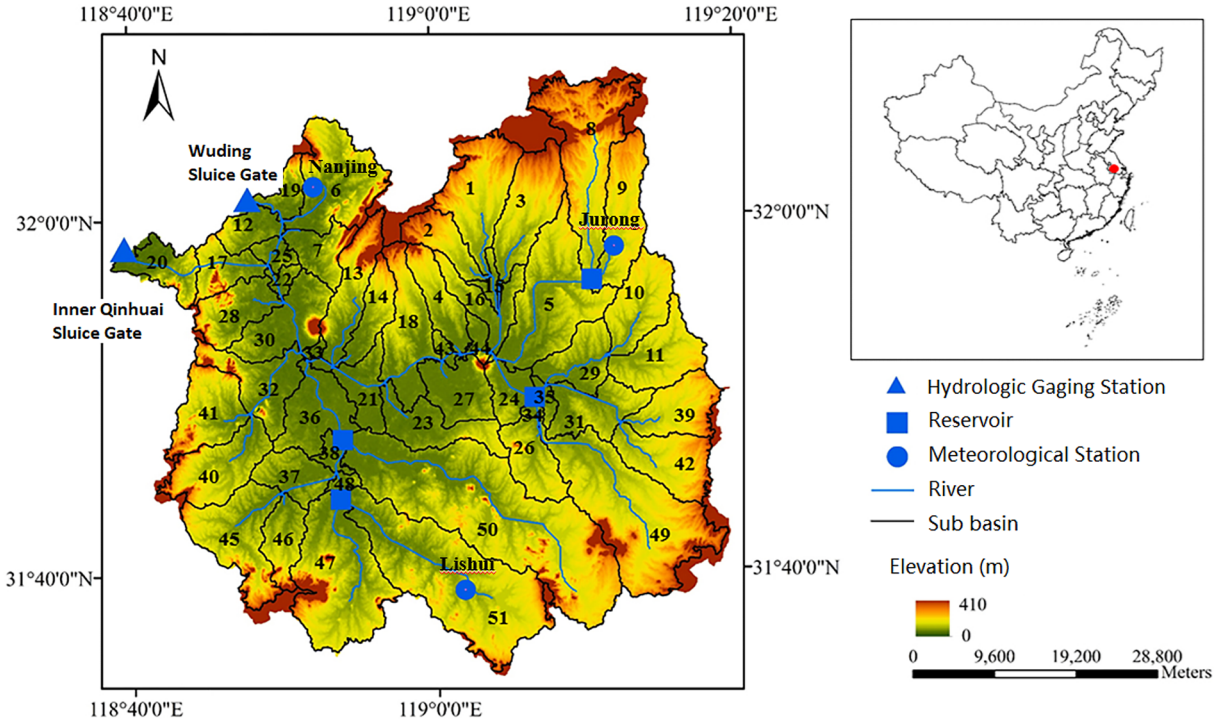

Fig. 1. Topography, river network, hydrometerological measurements in the Qinhuai River Basin (QRB) located in the humid southern China.

(Arnold et al., 2012). The entire watershed simulation domain is divided into sub-basins, which are further subdivided into uniform hydrological response units (HRUs) with homogeneous soil, land-cover, and slope characteristics. About 300 HRUs in 54 sub-basins were used in the present study. Simulations of hydrological processes such as ET and percolation occur at the HRUs level (Arnold et al., 2012; Gassman et al., 2007). The model parameters are distributed across HRUs and are finalized during model calibration and validation by comparing simulated and measured hydrologic fluxes including both streamflow and ET. In this study, we use the SCS method and Penman-Monteith equation for estimating surface runoff and PET, respectively. For estimating total actual ET at the HRUs level, SWAT first calculates plant canopy interception, then simulates the maximum amount of transpiration and soil evaporation, and computes the actual soil evaporation last.

2.3. Improved SWAT model

The original SWAT model treats a rice paddy as an impounded area (Xie and Cui, 2011). In this study, to represent flow patterns of a rice paddy landscape, we modified the SWAT wetland pothole module that is originally introduced by Sakaguchi et al. (2014) and Xie and Cui (2011). Additional modifications to SWAT include algorithms for estimating wetland surface area, irrigation schedules, and the evaporation process of pothole. (Fig. 2) (More supporting information see Appendix A, Figs. A.1–A.3).

2.3.1. Calculation of the surface area of rice paddy field

The surface area (*SA*) of the original pothole module is computed as a cone-shaped wetland which varies with the volume of water stored in the impoundment. The improved rice paddy model assumes that the surface area of rice paddy in the pothole module as a cuboid shape according to Sakaguchi et al. (2014). Thus, the surface area of water would not decrease with the decrease of water level. The equation of the surface area has been changed as follows:

$$SA = A_{HRU} SA = A_{HRU} \quad (1)$$

where A_{HRU} is the surface area of the HRU (ha) dominated by rice paddies.

2.3.2. Irrigation algorithms

The actual amount of irrigation is difficult to estimate since the timing of irrigation operations is often irregular, thus the original pothole module assumes enough water for irrigation without considering unused water. Therefore, this algorithm does not reflect the reality of the irrigation system in the study area. When the water storage in paddy field reaches its maximum after irrigation, the irrigation water becomes overflow. Therefore, this study assumes that the daily water need of irrigation by a rice paddy is equal to the rate of flow in the irrigation canal. The improved model for rice paddy field takes unused water into account by adding an irrigation formula preventing irrigation water overflowing the modelled impoundment:

$$if V_{pot} + irr > V_{mxpot}, irr_{pot} = V_{mxpot} - V_{pot} \quad (2)$$

$$if V_{pot} + irr \leqslant V_{mxpot} irr_{pot} = irr \quad (3)$$

where irr_{pot} is the amount of water added to the impoundment on a given day (m^3); V_{pot} is the current volume of water stored in the impoundment (m^3); V_{mxpot} is the maximum volume of water which can be stored in the impoundment (m^3); *irr* is the amount of water added through an irrigation operation on a given day (m^3).

Accordingly, the drainage process has been modified as:

$$if V_{pot} + irr > V_{mxpot}, Q_{out} = Q_{surf} + \frac{(V_{pot} + irr - V_{mxpot})}{(10A_{HRU})} \quad (4)$$

$$if V_{pot} + irr \leqslant V_{mxpot} Q_{out} = Q_{surf} \quad (5)$$

where Q_{out} is the volume of water flowing out of a HRU to the main channel on a given day (mm); Q_{surf} is the volume of the surface runoff released from a HRU to the main channel which does not include the irrigation water overflow from the impoundment on a given day (mm).

2.3.3. Water evaporation algorithms

For modelling ET for rice paddies, we adopted findings from Miyazaki et al. (2005) and Sakaguchi et al. (2014) that water evaporation is limited when leaf area index (LAI) of rice crop exceeds 4.0.

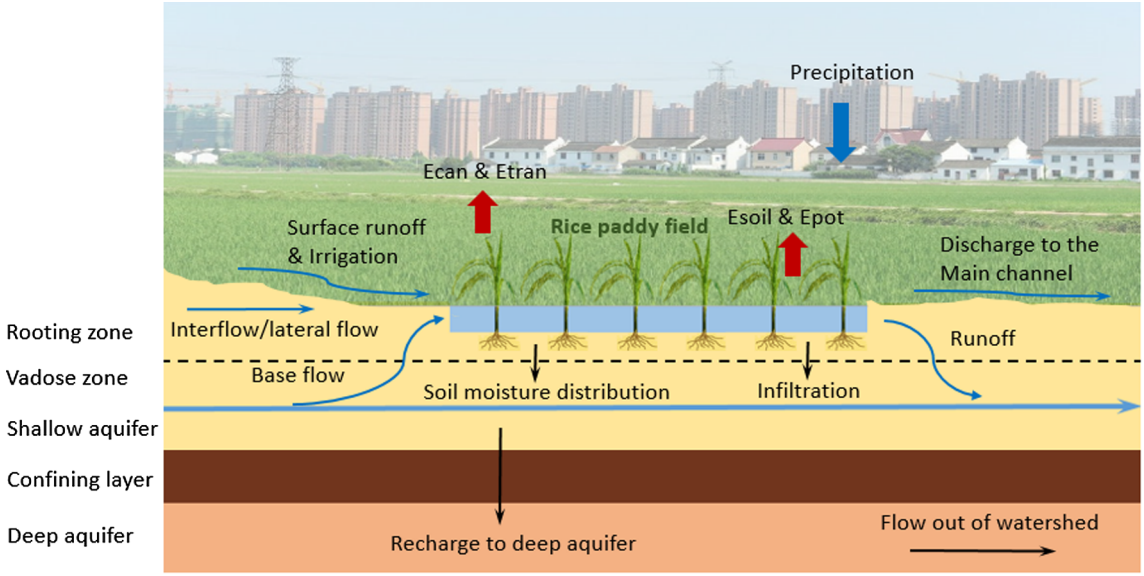

Fig. 2. Schematic diagram of the water balance in an improved paddy module (E_{can}, E_{tran}, E_{soil}, and E_{pot} denote the evaporation from free water in canopies, the crop transpiration, soil water, and impounded water surface of rice paddy, respectively).

In this case, more than 90% of the total ET is transpiration for rice paddy. This model modification ensures that rice transpiration depends on LAI and dominates ET. In addition, the evaporation coefficient η was introduced to estimate actual water evaporation based on PET. Thus, the ET equations were modified as:

$$ifLAI < 4,\ QUOTE V_{evap} = 10\eta \cdot (1 - LAI/4) \cdot PET \cdot SA(ifLAI < 4) V_{evap} = 10\eta \cdot (1 - LAI/4) \cdot PET \cdot SA(ifLAI < 4) \quad (6)$$

$$ifLAI \geq 4,\ QUOTE V_{evap} = 0(ifLAI \geq 4) V_{evap} = 0(ifLAI \geq 4) \quad (7)$$

where V_{evap} is the volume of water removed from the water body by evaporation per day (m^3); *PET* is the daily potential evapotranspiration (mm). In this study, we set η as 0.6 based on the evaporation process of the rice paddies (Neitsch et al., 2002).

2.4. Model input data

The data required to run SWAT consist of digital elevation model (DEM), land-cover, soil, and daily meteorological data (e.g. precipitation, relative air humidity, maximum and minimum temperature, solar radiation, and near surface wind speed). The 30 m × 30 m resolution DEM was obtained from the International Scientific Data Platform of the Chinese Academy of Sciences. We examined land use data for three distinct periods of 2000, 2004 and 2011. These spatial data were derived from Landsat Thematic Mapper (TM) and ETM + images with a 30 m × 30 m pixel resolution (http://glovis.usgs.gov/) (Fig. 3). The digital soil data at a 1:5,000,000 scale from the Harmonized World Soil Database (HWSD) updated by the Food and Agriculture Organization (FAO) of the United Nations and the International Institute for Applied Systems Analysis (IIASA) were used to extract soil information. The daily meteorological data for 27 years (1987–2013) were acquired from weather stations in/or near QRB and were interpolated to the DEM grids.

2.5. Parametrization for reservoir and irrigation management

SWAT provides several options related to water management practices that allow users to choose based on data availability such as irrigation, tile drainage, and consumptive water use. Water for irrigation in a HRU is obtained from one of the five main water sources: river reach, reservoir, shallow aquifer, deep aquifer, or a source outside the watershed. Reservoirs are impoundments located on the main channel network of the watershed. In this study, we added five reservoirs based on the reservoir information obtained from Nanjing Water Resources Bureau (Table 1). For rice paddy phonology, we set Jun 16th as the beginning day of the growing season, October 20th as the harvest day. In addition, November 2nd was set as the planting day, and May 20th as the harvest day of winter wheat rotation in the following year. The parameters for rice paddy irrigation operations were derived from local knowledge (Hao et al., 2015b; Huang et al., 2015; Wang et al., 2013; Wang et al., 2006), and the irrigation dates are listed in Table 2 (more information see Appendix B Table B.1).

2.6. Model performance evaluation and uncertainty analysis

Actual ET rates for a rice paddy field were measured by a weighing lysimeter at a research site with an area of 300 km^2 managed by the Agro-meteorological Experimental Station (32.21° N, 118.71° E) on the Nanjing University of Information Science and Technology (NUIST) campus, about 10 km from the QRB. The measurement period spanned from July 1st to November 2ndin 2007. The weather conditions at the NUIST station are similar to the Lishui Research Station dominated by rice paddy fields in the QRB. Therefore, the measured lysimeter ET rates were used to validate the simulated ET for rice paddy land covers. The precision of the ET measurements was estimated to be 0.1 mm day^{-1}. The effective ET area of the lysimeter was 4.0 m^2. Measured ET data in heavy rainy days were removed from the data sets due to potential estimation errors of the lysimeter method.

We used the Sequential Uncertainty Fitting Algorithm (SUFI-2) (Abbaspour et al., 2007) based on SWAT-CUP for parameter calibration and uncertainty analysis. A total of 10 parameters were chosen for calibration according to the sensitivity analysis method. Output uncertainty was calculated by the 95% prediction uncertainty (95PPU), which was defined as the interval between 2.5% and 97.5% levels of the cumulative distribution of simulated results (Zhao et al., 2015). The parameter uncertainty is one of the major sources of simulation uncertainty in modelling studies (Zhang et al., 2014). Two variables, *p*-factor and *r*-factor, were applied for defining parameter uncertainty. The *p*-factor was the percentage of observed data enveloped by the 95PPU, and *r*-factor indicated simulation accuracy. Theoretically, the *p*-factor ranges from 0 to 1 and *r*-factor ranges from 0 to infinity. When the *p*-factor is close to 0.7 and *r*-factor around 1 for discharge,

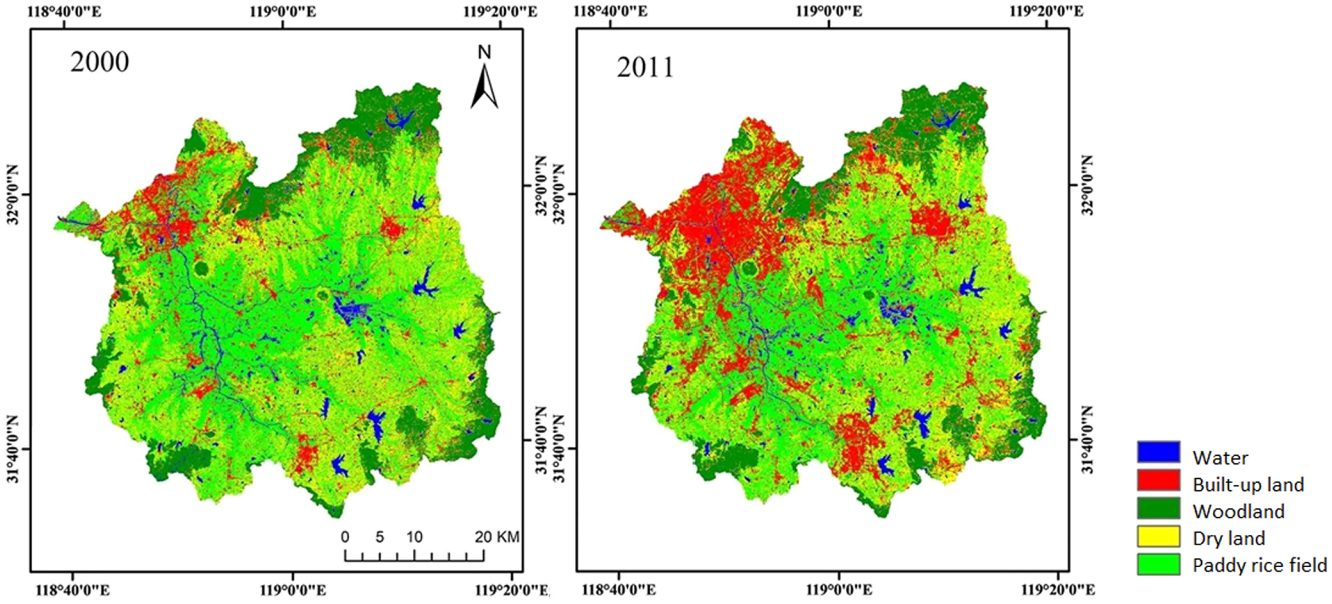

Fig. 3. Land covers and land uses of the Qinhuai River Basin (QRB) in 2000 and 2011.

Table 1
SWAT model parameters for five reservoirs in the Qinhuai River Basin (QRB).*

Reservoir	RES_ES[1]	RES_EVOL[2]	RES_PSA[3]	RES_PVOL[4]	RES_VOL[5]	RES_RR[6]
Beishan	188	5824	78	2601	192	250
Jurong	108	2002	64	1202	110	108
Chishanhu	719	6168	148	504	100	120
Fangbian	119	3106	74	2084	172	97
Zhongshan	81	2099	53	1318	137	95

* *Note*: [1]RES_ESA is reservoir surface area as determiend by water level at the emergency spillway (ha).
[2] RES_EVOL is volume of water needed to fill the reservoir to the emergency spillway (10^4 m^3).
[3] RES_PSA is reservoir surface area as determiend the principal spillway (ha).
[4] RES_PVOL is volume of water needed to fill the reservoir to the principal spillway (10^4 m^3).
[5] RES_VOL is initial reservoir volume (10^4 m^3).
[6] RES_RR is average daily principal spillway release rate (m^3 s^{-1}).

Table 2
SWAT model irrigation management parameters for rice paddy (RICE) in the Qinhuai River Basin (QRB).*

Crop	Starting Date	IRR_AMT[1]	IRR_EFM[2]	IRR_SQ[3]	FLOWMIN[4]	DIVMAX[5]
Rice	Jun 17th	20	0.75	0.1	100	150

* *Note*: Irrigation management is set as auto-irrigation operation in SWAT, and water for irrigation to an HRU is from rivers.
[1] IRR_AMT is the depth of irrigation water applied on an HRU (mm).
[2] IRR_EFM is the irrigation efficiency.
[3] IRR_SQ is the surface runoff ratio.
[4] FLOWMIN is the minimum in-stream flow for irrigation diversion (m^3 s^{-1}).
[5] DIVMAX is the maximum daily irrigation diversion from the reach (mm).

simulation outcomes are close to satisfactions. The years of 1987–1989 were selected as a warm-up period before the calibration period (1990–1994), and 1995–1999 was set as model validation. The land cover maps of 2000, 2004 and 2011 were used to represent three time periods of 2000–2003, 2004–2008 and 2009–2013 respectively.

The stream flow data were compiled from hydrologic records for the Wuding Sluice Gate hydrological station, which controlled the outflows from the Qinhuai River and back flows from the Yangtze River (Fig. 1). The monthly stream-flow data (1990–1999) used for model calibration and validation were the sum of daily flow measured at the Wuding Sluice Gate Station. The monthly data preprocessing and quality control were carried out by the local Jiangsu Bureau of Hydrology and Water Resources.

We applied three criteria to evaluate the model's performance in simulating streamflow: Nash-Sutcliffe model efficiency (*NSE*) (Nash & Sutcliffe, 1970; Moriasi et al., 2007), percent bias (PBIAS) (Gupta et al., 1999) and coefficient of determination (R^2) (Immerzeel et al., 2008) (see Appendix C). Values for R^2 range from 0 to 1, with 1 indicating a perfect linear relationship, and 0 indicating no linear relationship. Values for *NSE* between 0 and 1 are generally acceptable values for SWAT models (Moriasi et al., 2007). The optimal *PBIAS* value is 0, with lower values indicating accurate model simulation (Gupta et al., 1999; Paul et al., 2017).

2.7. Separating contributions of climate and LULCC to ET

We used the method developed by Eum et al. (2016) to estimate the individual contributions of LULCC and climate variability to the changes in ET. The period 1987–1999 was selected as the reference period with climate data from 1987 to 1999. Changes in ET were evaluated for three time periods of 2000–2003, 2004–2008 and 2009–2013 with climate data from 2000 to 2013 and LULCC representing three periods in 2000, 2004 and 2011, respectively. The effects of both LULCC and climate variability were determined from modelling results when changing LULCC from 2000 (simulated ET of 2000–2003) to 2004 (simulated ET of 2004–2008) then to 2011 (simulated ET of 2009–2011) with the entire weather data series (2000–2013). The individual contributions of LULCC or climate are

calculated by computing deviation of accumulated ET from the reference of LULCC or climate. Contribution of climate variability (E_c) during 2000–2013 was derived from ET values modelled by using fixed LULCC of 2000. Contribution of LULCC (E_l) represents ET derivation from the reference climate period (1987–1999). The accumulated ET deviation resulting from LULCC (E_{al}), climate variability (E_{ac}), and combined effects of climate change and LULCC (E_{acl}) were calculated as:

$$E_{cl}(t) = E(t) - \bar{E}_r E_{cl}(t) = E(t) - \bar{E}_r \quad (8)$$

$$E_c(t) = E_n(t) - \bar{E}_r E_c(t) = E_n(t) - \bar{E}_r \quad (9)$$

$$E_l(t) = E_{cl}(t) - E_c(t) E_l(t) = E_{cl}(t) - E_c(t) \quad (10)$$

$$E_{acl} = \sum_{t=2003}^{2013} E_{cl}(t) \quad (11)$$

$$E_{ac} = \sum_{t=2003}^{2013} E_c(t) \quad (12)$$

$$E_{al} = \sum_{t=2003}^{2013} E_l(t) \quad (13)$$

where $E_m(t)$ represent modelled annual ET rate at year t (t = 2003, 2004, …0.2013) using actual climate and LULC of the three representative periods. In particular, $E_m(t)$ rates in 2003 were estimated using LULCC of 2000 while $E_m(t)$ rates for 2004–2008 and 2009–2013 were simulated with LULCC of 2004 and 2011, respectively; $\bar{E}_r$ is the mean ET for the reference period of 1990–2002 with LULCC set as year 2000 and climate of the reference period; $E_{cl}(t)$ represents the combined ET effects of climate and LULCC for year t. $E_n(t)$ is modelled annual ET for year t during 2003–2013 with a fixed LULCC set as 2000. Therefore, $E_c(t)$ represents the sole effects of climate on ET for year t. E_{acl}, E_{ac}, and E_{al}, represents the accumulated effects of combined climate and land use change, accumulated effects of climate alone, and accumulated effects of land use alone by year t (t = 2003–2013), respectively.

The relative contributions of LULCC, $R_l(t)$, and climate variability, $R_c(t)$, at year t were calculated as:

$$R_l(t) = \frac{|E_l(t)|}{|E_l(t)| + |E_c(t)|} \quad (14)$$

$$R_c(t) = \frac{|E_c(t)|}{|E_l(t)| + |E_c(t)|} R_c(t) = \frac{|E_c(t)|}{|E_l(t)| + |E_c(t)|} \quad (15)$$

3. Results

3.1. Sensitivity analysis

Five iterations were used in model calibration to match simulated daily streamflow with measured at Wuding Sluice Gate, and each iteration was run for 500 times. The ten most sensitive parameters, as ranked according to model sensitivity from high to low, were identified (Table 3). In this study, the value of p-factor that represents the percentage of observed streamflow falling within the 95PPU of the simulated values, was 0.78 in the calibration period (1990–1994). In the meantime, the r-factor is 1.07, implying that the model results are acceptable (Abbaspour et al., 2007).

3.2. Model calibration and validation with measured streamflow and ET

When the original SWAT model was first tested, negative correlations between the observed and simulated streamflow were found, suggesting poor model performance of the default model. *NSE* values were lower than 0 both in 1990–1994 (*NSE* = −3.28) and 1995–1999 (*NSE* = −8.42), and the simulated value were much higher than the observations (Fig. 4). However, the improved SWAT model showed much better performance after model calibration and validation. Both *NSE* and R^2 exceeded 0.8 (*NSE* = 0.86, R^2 = 0.88), and *PBIAS* is less than 5% (−1.5%) on calibration period (1990–1994). As for validation period (1995–1999), *NSE* and R^2 for monthly streamflow simulation were 0.65 and 0.71, respectively, while *PBIAS* was only 0.07%. Furthermore, the simulated mean annual streamflow was 15.8 ($m^3\ s^{-1}$) and 13.3 ($m^3\ s^{-1}$) during calibration and validation period, respectively. The simulated high flows were compared well with measurements during spring and summer periods except in 1990 and 1994. Underestimates were noticed during winter and overestimates were obvious during autumn months except in 1993. Overall, the model performance indicators and simulated streamflow patterns suggested that the improved model performance was suitable for simulating major components of water balance for this watershed.

Table 3
Key SWAT model parameters and fitted values.*

Rank	Parameter	Variation	Range	Fitted value
1	CN2	Absolute	−30 to 0	−24
2	ALPHA_BF	Absolute	0 to 0.002	0.001
3	ESCO	Replace	0.01 to 1	0.043
4	SOL_AWC	Relative	−0.03 to 1	0.98
5	SOL_Z	Absolute	−17 to 80	47.9
6	EPCO	Replace	0.01 to 1	0.78
7	GWQMN	Replace	2000 to 4500	3345
8	REVAPMN	Replace	0 to 450	35
9	GW_DELAY	Replace	0 to 500	1
10	CANMX	Replace	0 to 100	85

* Note: Relative means of an existing parameter value are multiplied by the (1 + a given value), Replace means the default parameter is replaced by the given value, and Absolute means the given parameter value is added to the existing parameter value. CN2 is SCS runoff curve number for moisture condition II. ALPHA_BF is baseflow alpha factor characterizes the groundwater recession curve. ESCO is soil evaporation compensation coefficient. SOL_AWC is available water capacity of the soil layer (mm). SOL_Z is depth from soil surface to bottom of layer (mm). EPCO is plant uptake compensation factor. GWQMN is threshold depth of water in the shallow aquifer required for return flow to occur (mm). REVAPMN is threshold depth of water in the shallow aquifer for "revap" to occur (mm). GW_DELAY is groundwater delay. CANMX is Maximum canopy storage.

The daily measured and modelled ET rates showed a good agreement as determined by a regression model with a slope of 0.75 and a coefficient of determination (R^2) of 0.75 (Fig. 5). The average of the ET measurement is 4.0 mm during the observation period from May 2007 to November 2007. The estimated ET is 3.8 mm, and its relative error is − 5.8%, on average. This was an improvement when compared with the original modelling results (R^2 = 0.49, negative slope).

3.3. Monthly variations and temporal trend of PET, VPD, and ET at watershed scale

At the monthly scale, modelled ET and PET as well as vapour pressure deficit (VPD) showed consistent variations (Fig. 6). The pattern was mainly attributed to the combination of temperature and precipitation variations. The ET and PET rates peaked in August and July due to high precipitation and air temperature during this period. Relative low values of ET and PET occurred in June were mostly attributed to increased relative humidity in the plum rainy season lasting for about 30–40 days from the end of May to early July. In general, variations of ET, PET and VPD follow similar seasonal patterns at the monthly scale.

The slopes of the ET trend lines for the growing season, Spring, Summer, Autumn, and Winter, were all negative with values of −2.68, −0.36, −1.01, −2.03, and −1.30, respectively. ET rates decreased in all seasons, and annual ET reduction mostly occurred during the growing season (Fig. 7a). However, the slopes of the trend regression lines for PET had all positive values of 5.50, 4.47, 4.22, 2.32, and 1.57

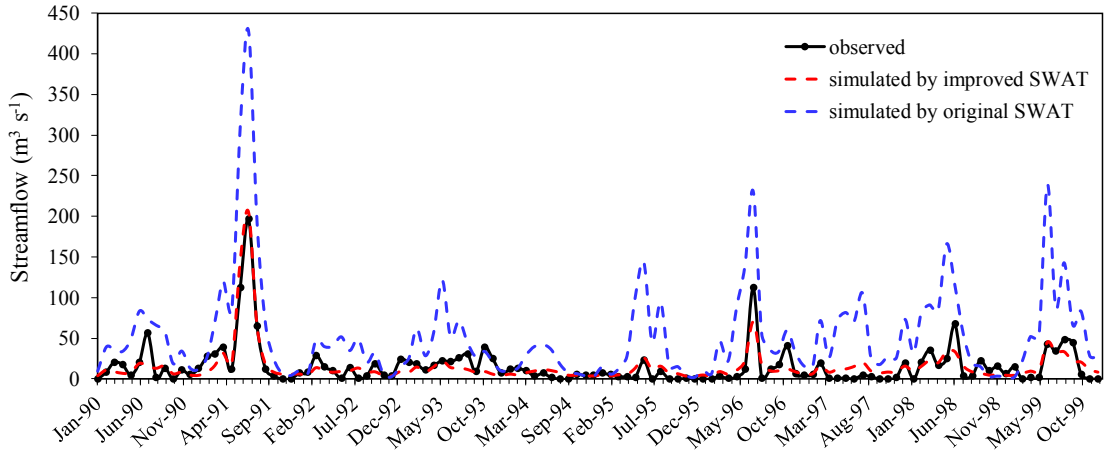

Fig. 4. Comparison of the observed monthly streamflow, simulated results by the improved and the original SWAT model ($m^3\ s^{-1}$) at Wuding Sluice Gate over the calibration period (1990–1994) and validation period (1995–1999).

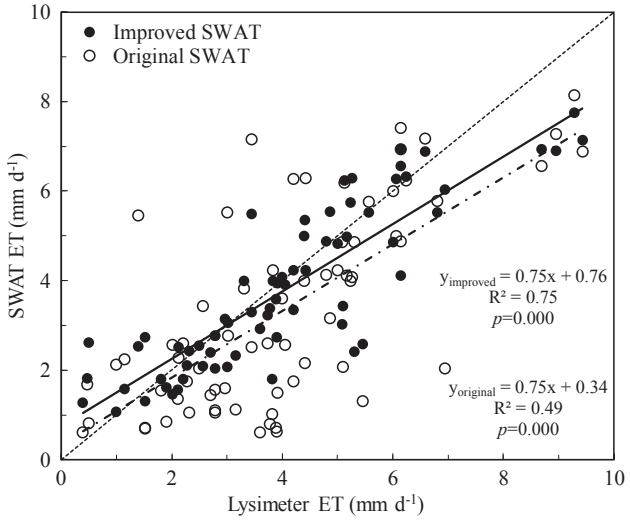

Fig. 5. A comparison of simulated evapotranspiration (ET) by the improved and the original SWAT model with measurements by a lysimeter method in a paddy rice field in 2007.

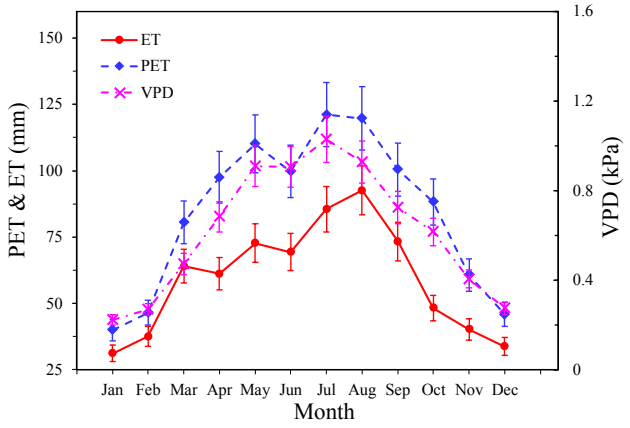

Fig. 6. Estimated mean watreshed-scale monthly evapotranspiration (ET), potential ET (PET), and Vapor Pressure Deficit (VPD) during 2000–2013 (the vertical lines show standard deviations) for the Qinhua River Basin (QRB).

for the growing season, Spring, Summer, Autumn, and Winter, respectively. PET increased significantly in all seasons, especially the growing season, Spring, and Summer. VPD showed an increasing trend during the 14-year study period, consistent with PET trend, but with an opposite trend of ET.

3.4. Annual trend of ET at watershed scale and contributions of LULCC

Overall, simulated annual actual ET at the watershed scale decreased from 2000 to 2013. This was in contrary to simulated PET. PET increased due to an increase in air temperature (Fig. 7b). Annual ET rates decreased from 700 mm in 2000 to 627 mm in 2004 (3.4% reduction), and then dropped to a minimum value of 524 mm in 2011 (19.4% reduction), while annual watershed-level PET increased from 942 mm to 1034 mm (9.6% increase) and further jumped to 1164 mm (20.4% increase) subsequently. Meanwhile, precipitation (P) increased from 2000 to 2010, contrary to the observably decrease trend of ET during the same period. Runoff coefficient of Q/P increased from 0.40 (2000) to 0.52 (2013), while the ratio of ET/P reduced by 14% (2000–2011).

Rice paddy field (RICE) contributed most to watershed ET volume (m^3), ranging from 46% up to 56%, followed by agricultural land (AGRC) 27 − 31%) (Fig. 8). An obvious increasing trend of ET contribution by urban lands (URHD, 9%) agreed with urban area expansion that mainly involved land conversion from crop land especially rice paddy (decreased by 6.8% in area), while forest (FRST) ET remained unchanged owing to the small change (only 1.2%) in total area.

3.5. Contrasting trend of ET and PET by LULCC at field (HRU) level

HRUs with little changes in LULCC (Fig. 9) showed that ET rates in agricultural land (AGRC), urban use (URHD), forest (FRST) and rice paddy (RICE) increased by 7.3%, 12.9%, 26.4% and 12.5%, respectively. The findings were consistent with the increasing trend of PET due to global warming. PET with urban use was much higher than that of other land cover types. Forests showed higher ET than other land cover types, followed by rice paddy fields, and agricultural land, and ET rates in urban areas were the lowest.

3.6. Relative contributions of climate change and LULCC to long term total ET variations

Our previous study has identified a streamflow 'break point' of 2003 showing a dramatic increase in streamflow during 2003–2013 due to LULCC (Hao et al., 2015a). Thus, the period of 2003–2013 was selected to separate the contributions of LULCC and climate change to total ET change. The accumulated contributions of LULCC (E_{al}) and climate variability (E_{ac}) to the simulated ET change appeared to be in opposite directions (Fig. 10). The contribution of climate to change in ET was

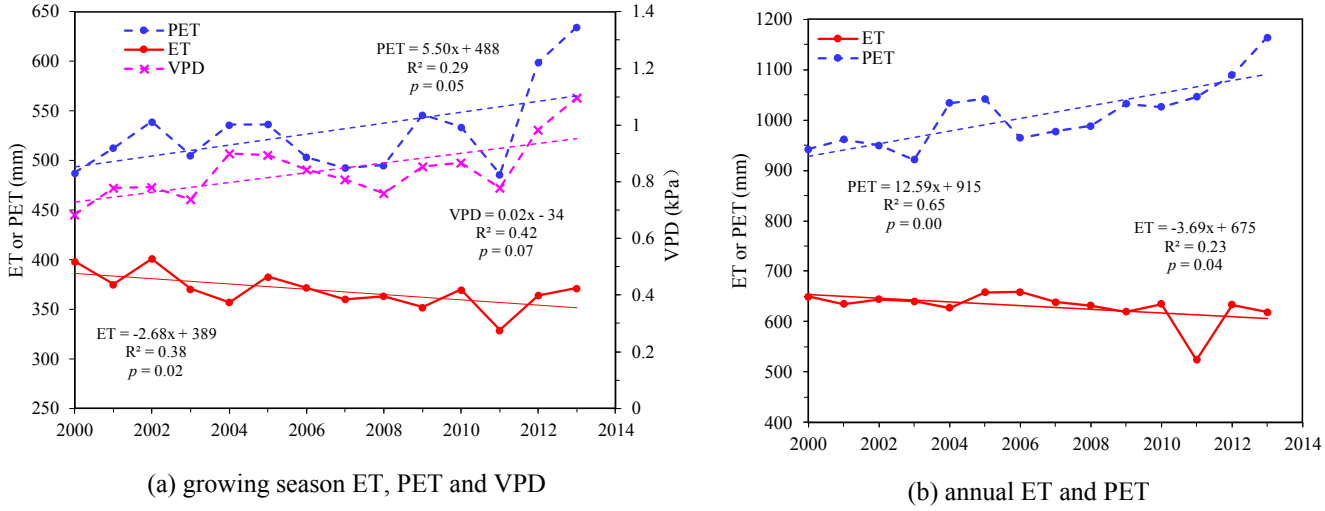

Fig. 7. Simulated watershed-scale (a) growing season evapotranspiration (ET), potential ET (PET) and Vapor Pressure Deficit (VPD) for rice paddies; (b) annual ET and PET during 2000–2013 with all different land use and covers. Land use and land covers of 2000, 2004, and 2011were used for the period of 2000–2003, 2004–2008, and 2009–2013, respectively.

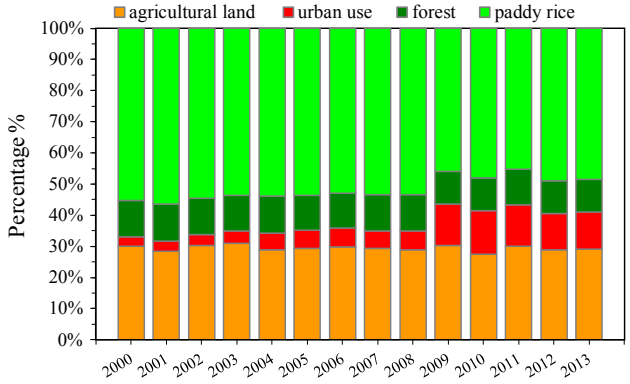

Fig. 8. The relative contributions of each land cover type to total evapotranpiration (ET) in the Qinhuai River Basin (QRB).

positive (29%), while the contribution of LULCC was negative (−50%). Overall, the combined accumulated contributions of climate and LULCC caused the annual ET to decrease by − 21% (E_{acl}) (Fig. 10). Dynamic attribution analysis indicated that the negative contribution of LULCC (R_l) to change in ET increased from 53% in 2000 to 61% in 2013 while the positive contribution of climate variability (R_c) decreased from 47% in 2000 to 39% in 2013. This demonstrated that land-cover change was the main driver of change in watershed-level ET during the study period (insert in Fig. 10).

4. Discussion

4.1. Impacts of climate change on PET, ET

Our study results were consistent with the literature regarding the relationship among ET, PET, and climate warming for humid regions. Because temperature and relative humidity are the two key factors effecting PET and ET variation (Yang, 2014; Mcleod et al., 2004; Yang et al., 2014; Wang et al., 2016; Gong et al., 2006; Feng et al., 2017) especially in humid areas (Feng et al., 2016; Liu et al., 2010), any rise in air temperature is likely to increase PET. Our previous studies (Hao et al., 2015a; Qin et al., 2019) and Gong et al. (2006) suggested that the increase in PET is mainly due to the increase in air temperature or global warming followed by the increase in VPD and decrease in relative humidity (RH). VPD is an important factor determining ET process by affecting canopy-level evaporation and leaf-level transpiration (Wu et al., 2015; Silva et al., 2016). We showed that PET and VPD had an upward tendency, contrary to the notable decreasing trend of actual ET over the past 14 years. We also found that precipitation increased during this period from 2000 to 2010. However, ET decreased at the watershed level. The increasing trends of PET and precipitation indicated that the decrease in ET trend was not likely to be caused by climate change at the watershed scale.

4.2. Impacts of Land-Use and Land-Cover change (LULCC) on ET

The relative contributions of LULCC and climate (Fig. 10) showed that watershed-level ET reduction was not only influenced by climate change, but also was strongly affected by LULCC. This was consistent with our previous streamflow attribution analysis based on two empirical models in the same watershed (Hao et al., 2015a). We found that LULCC contributed about 85% of the observed increase in streamflow and climate variability of precipitation contributed about only 15%. Therefore, the current method is acceptable to separate the hydrological impacts of climate variability from land-use/land-cover change with the aid of the SWAT model. The results support our hypothesis that land-use/land-cover change is the main driver to ET variations.

4.3. Factors affecting change in ET at different spatial scales

Most previous studies on the QRB focused on temporal variations in streamflow (Du et al., 2012; Du et al., 2013; Liu et al., 2012), and recently on ET (Hao et al., 2015a; Zheng et al., 2020) at the watershed level. The current study focused on the spatial distribution of ET of different land-cover types. In our study, at HRU scale, ET of all land-cover types is increasing significantly, especially for forest and rice paddy field (Fig. 9). The ET increase patterns were similar to increasing PET which was mainly influenced by increasing air temperature, VPD and RH from 2000 to 2013. Among all land covers, ET rates from forests were highest due to their high canopy interception and transpiration rates. Therefore, ET variations were dominated by meteorological factors and plant types at the HRU scale. However, for watershed scale, the volume of ET for rice paddy and agricultural lands were decreasing, causing overall decrease in ET at the watershed level. Therefore, LULCC plays a critical role in affecting the hydrology at the watershed scale.

4.4. Impacts of LULCC on streamflow as a result of reduction of ET

Numerous studies show that urbanization leads to increase in water

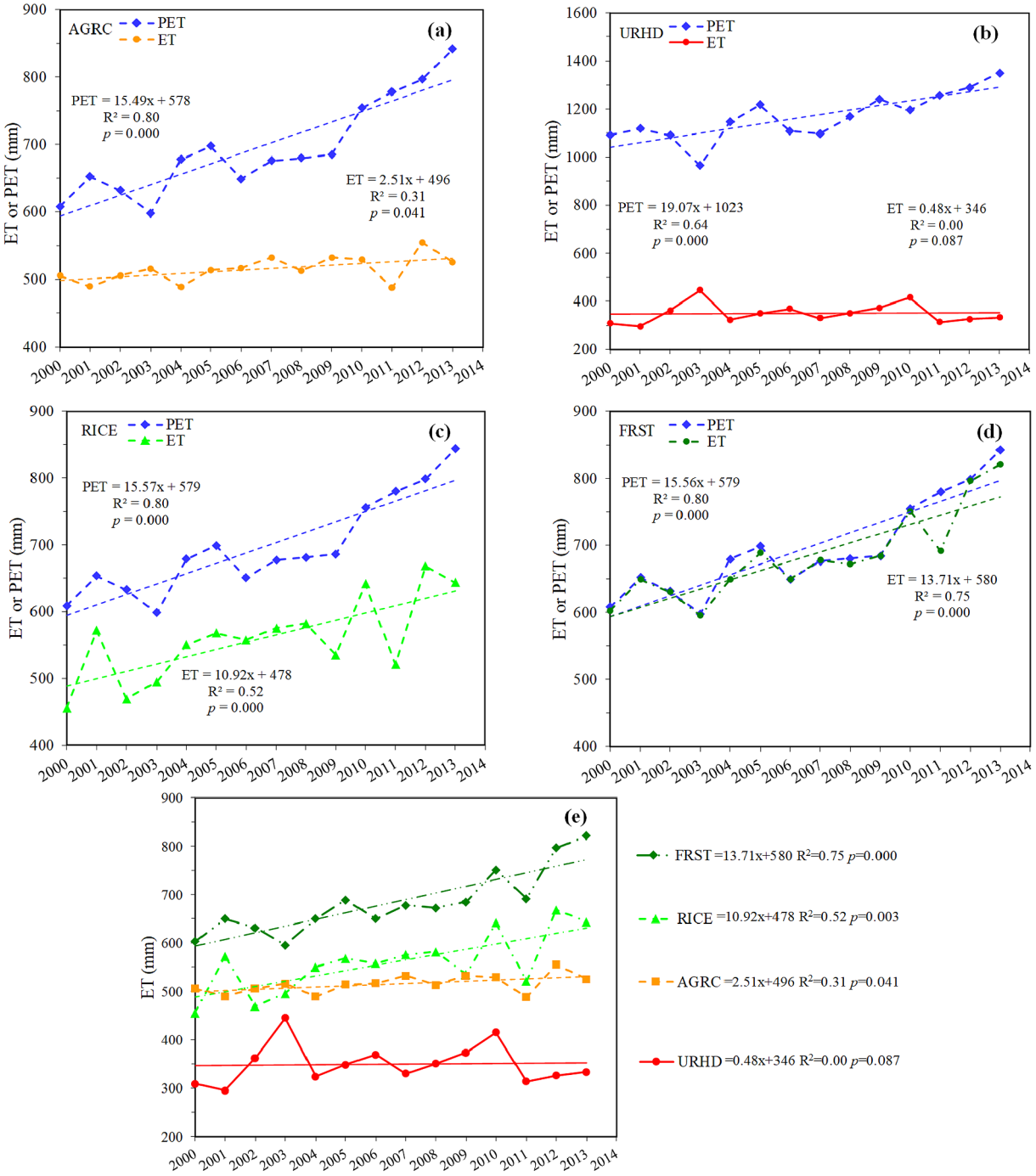

Fig. 9. Simulated annual ET and PET at the hydrological response units (HRUs) scale with little land cover change in the Qinhuai River Basin. (a) AGRC: agricultural land, (b) URHD: urban use, (c) RICE: paddy rice, and (d) FRST: forest, (e) HRU ET with different land cover types.

yield as a result of increase in direct runoff from impervious surfaces (Oudin et al., 2018; Li et al., 2020) and decrease in ET (Boggs and Sun, 2011) due to reduction in canopy interception, lower soil percolation rate and soil moisture storage capacity (Locatelli et al., 2017; Xu et al., 2017; Barron et al, 2013; Zhou et al., 2013; Nguyen and Kappas, 2015; Lin et al., 2015; Baker and Miller, 2013; Nie et al.,2011; Zhu and Li, 2014). Our simulated results support these findings. LULCC during 2000–2013 in the QRB increased annual total streamflow when calculated as Q = P − ET with a decrease in ET and a slight increase in P. The reduction of watershed-level annual ET is mostly resulted from converting rice paddy to urban uses. The rice paddy represents the largest area of the whole watershed and contributes most to ET comparing with other land-cover types (Fig. 8). The relatively high level of R^2 and low p value in growing season (Fig. 7) also show agreement with the fact that reduced ET in rice paddy is the main contributor to total ET decrease. Du et al. (2012) reported that annual runoff as well as flood volume would increase with increase in impervious area by urbanization in the QRB. Other studies (Xu et al., 2017; Zhou et al., 2013) pointed out that land-cover change would alter soil property which dramatically change the soil moisture storage capacity and infiltration rate. Kim et al. (2014) applied the HSPF-Paddy model in Bochung watershed of Korea and found that runoff depth and ET from rice paddy field were higher than other land-cover types attributed to amounts of water irrigation. Feng and Liu (2015) indicated

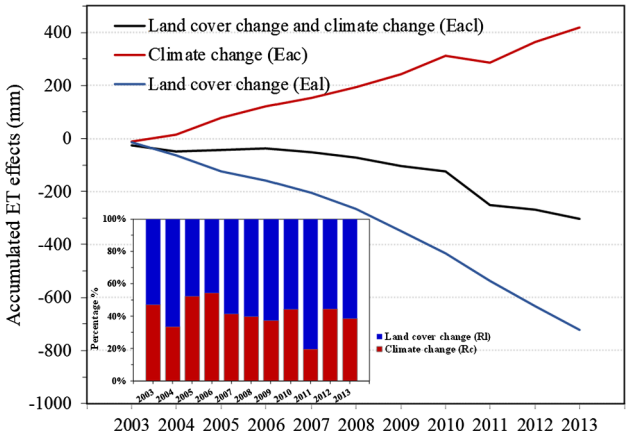

Fig. 10. Accumulated ET effects due to land cover change (E_{al}) and climate change (E_{ac}), as well as accumulated ET effects resulting from both land cover change and climate change (E_{acl}). The insert shows the relative contribution of land cover change (R_l) and climate change (R_c) to annual ET respectively in the Qinhuai River Basin during 2003–2013.

that soil moisture change is mainly controlled by land-cover types in humid area of Poyang Lake Basin, China.

4.5. Implications of urbanization to watershed ecosystem services and climate feedback

Paddy wetlands are the main land use type across the humid southern China. Our study shows that LULCC, reduction of paddy rice field due to urbanization in particular, alters the watershed hydrological cycle. Such hydrologic changes have important implications to flooding risks due to increase in storm runoff and water quality degradation from sediment and urban runoff (Sun and Lockaby, 2012). Because the water and energy is tightly coupled, reduction in wetlands including rice paddies is likely to aggravate Urban Heat Island effect (Zhou et al., 2013) and Urban Dry Island effect (Hao et al., 2018) in the study region. Thus, paddy field not only provide abundant agricultural resources, but also play a key role in local climate regulation, soil and water conservation, water storage and flood regulation, groundwater supply, water purification, and local and global geochemical cycle (e.g., Greenhouse Gas emission that depends in hydrology). The feedbacks of the ecohydrological cycle to urbanization-associated land cover change are particularly evident in subtropical humid regions such as southern China that are dominated by water bodies and wetlands including rice paddy fields or extensive wetlands and forests. However, the ecosystem service functions of these artificial wetlands are being threatened by massive urbanization in southern humid China (Tsai 2002; He et al. 2009).

In this study, the traditional watershed ecohydrological simulation model (SWAT) was improved and adapted for the paddy field-dominated basin. The present watershed-level study advances our understanding of the combined and individual impacts of land use/land cover change and climate change on watershed ecohydrological processes at multiple spatial scales. The process-based study at multiple scales offers insight of hydrological response to urbanization and our findings have important environmental implications for integrated watershed management (i.e., both climate and LULCC). The improved model provides a better integrated method for ecosystem services assessment in the highly urbanized regions in humid southern China and East Asia.

4.6. Uncertainties and limitations

Parameter uncertainty is one of the major sources resulting in the hydrological simulation uncertainty (Zhao et al., 2015; Zhang et al., 2014). Monthly streamflow during 1990–1999 from Wuding Sluice Gate is the only data used for model calibration and validation, thus leading to range of deviation in parameters for the subbasins. A lack of the observed streamflow and ET in subbasins can result in bias in calibrated parameters. Studies by Xie and Cui (2011) have incorporated with new paddy module in SWAT by introducing three critical water depths designed for irrigation and drainage management during the rice paddy growing period in China, indicating that simulated results showed a good agreement with the measurements. However, the improved irrigation algorithm of the pothole module is not able to completely represent actual irrigation process because the volume of irrigation varies with different growth stage of rice paddy and is affected by local artificial irrigation plans. In addition, the modified model does not account for the infiltration as affected by soil types (Kang et al., 2006) and ground water level of the drainage channel (Sakaguchi et al., 2014). Combining with physically based ground water models with surface water processes will likely to improve the SWAT model further for application in a humid region (Kim et al., 2008). Similar to previous work (Sakaguchi et al., 2014), our study provides critical information and strategies for improving rice paddy module for understanding hydrological process in a rice paddy dominated region. The improved SWAT model still needs to be evaluated in other watersheds for ET in similar landscape in the future when field data (such as FLUXNET) (Liu et al., 2017b) become available at different spatial scales. The impacts of shallow groundwater on ET and streamflow should be explicitly modeled in future studies. This is important for humid regions where ET is closely couple with surface and groundwater systems, and wetland dynamics (Lu et al., 2009; Dai et al., 2010).

5. Conclusions

We quantified the response of ET to LULCC associated with rapid urbanization and climate change over a 14-year period in the Qinhuai River Basin, southern China. We conclude that the driving factors to ET change vary with spatial scale. Conversion of cropland to urban use directly results in significant ET reduction and increase in runoff at a watershed scale in spite of a warming climate and rise of water evaporation demand.

Replacing the original wetland and irrigation algorithms with new models describing the hydrological processes for rice paddy greatly improved SWAT model performance. Integrating multiple methods and techniques of ecohydrological model, ground observation and remote sensing to study the effects of land-use/land-cover change on ecological processes (e.g. ET) is essential and beneficial for explaining the mechanisms regulating of hydrological processes in a rapidly urbanizing watershed.

To mitigate the environmental effects of urbanization such as flooding, water quality degradation, Urban Heat Island, and Urban Dry Island in southern China, future impacts from changes in global climate and land use change must be managed together along with ecosystem conservation measures. The improved SWAT provides a useful modelling tool for ecosystem service impact assessment and land planning in the rapidly urbanizing regions in southern China.

CRediT authorship contribution statement

Di Fang: Conceptualization, Methodology, Software, Validation, Writing - original draft. **Lu Hao:** Conceptualization, Methodology, Software, Validation, Writing - original draft. **Zhen Cao:** Data curation, Visualization, Investigation. **Xiaolin Huang:** Data curation, Visualization, Investigation. **Mengsheng Qin:** Data curation, Visualization, Investigation. **Jichao Hu:** Data curation, Visualization, Investigation. **Yongqiang Liu:** Supervision, Writing - review & editing. **Ge Sun:** Supervision, Writing - review & editing.

Declaration of Competing Interest

The authors declare that they have no known competing financial interests or personal relationships that could have appeared to influence the work reported in this paper.

Acknowledgments

This work was supported by the National Natural Science Foundation of China (grant numbers 41877151, 41571026, and 41977409) and China Meteorological Administration (CMA)/Henan Key Laboratory of Agrometeorological Support and Applied Technique (grant numbers AMF201410). We thank China Meteorological Administration, Jiangsu Meteorological Bureau for their assistance in data sharing and Sakaguchi et al. for their useful advice on rice paddy module improvement. Partial support was also received from the Southern Research Station, USDA Forest Service.

Appendix A. Supplementary data

Supplementary data to this article can be found online at https://doi.org/10.1016/j.jhydrol.2020.124869.

References

Abbaspour, K. C., Vejdani, M., and Haghighat, S., 2007. SWAT-CUP calibration and uncertainty programs for SWAT. Modsim International Congress on Modelling & Simulation Land Water & Environmental Management Integrated Systems for Sustainability, 364, 1603–1609.

Abdullah, S.S., Malek, M., Abdullah, N.S., Kisi, O., Yap, K.S., 2014. Extreme learning machines: a new approach for prediction of reference evapotranspiration. J. Hydrol. 527, 184–195.

Amatya, D., Sun, G., and Gowda, P., 2014. Evapotranspiration: Challenges in Measurement and Modeling. Eos Transactions American Geophysical Union, 95, 256–256.

Aouissi, J., Benabdallah, S., Chabaâne, Z.L., Cudennec, C., 2016. Evaluation of potential evapotranspiration assessment methods for hydrological modelling with SWAT—Application in data-scarce rural Tunisia. Agric. Water Manage. 174, 39–51.

Arnold, J.G., Moriasi, D.N., Gassman, P.W., Abbaspour, K.C., White, M.J., Srinivasan, R., Santhi, C., Harmel, R.D., Griensven, A.V., Liew, M.W.V., 2012. SWAT: Model use, calibration, and validation. Trans. ASABE 55, 1549–1559.

Baker, T.J., Miller, S.N., 2013. Using the Soil and Water Assessment Tool (SWAT) to assess land use impact on water resources in an East African watershed. J. Hydrol. 486, 100–111.

Barron, O.V., Barr, A.D., Donn, M.J., 2013. Effect of urbanisation on the water balance of a catchment with shallow groundwater. J. Hydrol. 485, 162–176.

Boggs, J., Sun, G., 2011. Urbanization alters watershed hydrology in the Piedmont of North Carolina. Ecohydrology 4, 256–264.

Brath, A., Montanari, A., Moretti, G., 2006. Assessing the effect on flood frequency of land use change via hydrological simulation (with uncertainty). J. Hydrol. 324, 141–153.

Cao, L., Zhang, Y., Shi, Y., 2011. Climate change effect on hydrological processes over the Yangtze River basin. Quat. Int. 244, 202–210.

Chien, H., Yeh, P.J.-F., Knouft, J.H., 2013. Modeling the potential impacts of climate change on streamflow in agricultural watersheds of the Midwestern United States. J. Hydrol. 491, 73–88.

Chirouze, J., Boulet, G., Jarlan, L., Fieuzal, R., Rodriguez, J., Ezzahar, J., Raki, S.E., Bigeard, G., Merlin, O., Garatuza-Payan, J., 2014. Intercomparison of four remote-sensing-based energy balance methods to retrieve surface evapotranspiration and water stress of irrigated fields in semi-arid climate. Hydrol. Earth Syst. Sci. Discuss. 1165–1188.

Cristiano, P.M., Campanello, P.I., Bucci, S.J., Rodriguez, S.A., Lezcano, O.A., Scholz, F.G., Madanes, N., Francescantonio, D.D., Carrasco, L.O., Zhang, Y.J., 2015. Evapotranspiration of subtropical forests and tree plantations: A comparative analysis at different temporal and spatial scales. Agric. For. Meteorol. 203, 96–106.

Crooks, S., Davies, H., 2001. Assessment of land use change in the Thames catchment and its effect on the flood regime of the river. Phys. Chem. Earth Part B 26, 583–591.

Dai, Z., Li, C., Trettin, C., Sun, G., Amatya, D., Li, H., 2010. Bi-criteria evaluation of the MIKE SHE model for a forested watershed on the South Carolina coastal plain. Hydrol. Earth Syst. Sci. 14, 1–14.

Du, J., Qian, L., Rui, H., Zuo, T., Zheng, D., Xu, Y., Xu, C.-Y., 2012. Assessing the effects of urbanization on annual runoff and flood events using an integrated hydrological modeling system for Qinhuai River basin, China. J. Hydrol. 464, 127–139.

Du, J., Rui, H., Zuo, T., Li, Q., Zheng, D., Chen, A., Xu, Y., Xu, C.Y., 2013. Hydrological simulation by SWAT model with fixed and varied parameterization approaches under land use change. Water Resour. Manage. 27, 2823–2838.

Eum, H.I., Dibike, Y., Prowse, T., 2016. Comparative evaluation of the effects of climate and land-cover changes on hydrologic responses of the Muskeg River, Alberta, Canada. J. Hydrol. Reg. Stud. 8, 198–221.

Falamarzi, Y., Palizdan, N., Huang, Y.F., Lee, T.S., 2014. Estimating evapotranspiration from temperature and wind speed data using artificial and wavelet neural networks (WNNs). Agric. Water Manage. 140, 26–36.

Fan, M., Shibata, H., Wang, Q., 2016. Optimal conservation planning of multiple hydrological ecosystem services under land use and climate changes in Teshio river watershed, northernmost of Japan. Ecol. Ind. 62, 1–13.

Feng, H., Liu, Y., 2015. Combined effects of precipitation and air temperature on soil moisture in different land covers in a humid basin. J. Hydrol. 531, 1129–1140.

Feng, Y., Cui, N., Zhao, L., Hu, X., Gong, D., 2016. Comparison of ELM, GANN, WNN and empirical models for estimating reference evapotranspiration in humid region of Southwest China. J. Hydrol. 536, 376–383.

Feng, Y., Jia, Y., Cui, N., Zhao, L., Li, C., Gong, D., 2017. Calibration of Hargreaves model for reference evapotranspiration estimation in Sichuan basin of southwest China. Agric. Water Manage. 181, 1–9.

Gao, J., Sang, Y., 2017. Identification and estimation of landslide-debris flow disaster risk in primary and middle school campuses in a mountainous area of Southwest China. Int. J. Disaster Risk Reduct. 25, 60–71.

Gao, X.J., Zhao, Z.C., Giorgi, F., 2002. Changes of extreme events in regional climate simulations over East Asia. Adv. Atmos. Sci. 19 (5), 927–942.

Gassman, P.W., Reyes, M.R., Green, C.H., Arnold, J.G., 2007. The soil and water assessment tool: historical development. Appl. Future Res. Direct. 50, 1211–1250.

Gong, L., Xu, C.Y., Chen, D., Halldin, S., Chen, Y.D., 2006. Sensitivity of the Penman-Monteith reference evapotranspiration to key climatic variables in the Changjiang (Yangtze River) basin. J. Hydrol. 329, 620–629.

Gu, C., Hu, L., Zhang, X., Wang, X., Guo, J., 2011. Climate change and urbanization in the Yangtze River Delta. Habitat Int. 35, 544–552.

Gupta, H.V., Sorooshian, S., Yapo, P.O., 1999. Status of automatic calibration for hydrologic models: comparison with multilevel expert calibration. J. Hydrol. Eng. 4, 135–143.

Guo, H., Hu, Q., Jiang, T., 2008. Annual and seasonal streamflow responses to climate and land-cover changes in the Poyang Lake basin, China. J. Hydrol. 355, 106–122.

Hao, L., Sun, G., Liu, Y., Wan, J., Qin, M., Qian, H., Liu, C., Zheng, J., John, R., Fan, P., 2015a. Urbanization dramatically altered the water balances of a paddy field-dominated basin in southern China. Hydrol. Earth Syst. Sci. 19, 3319–3331.

Hao, L., Sun, G., Liu, Y., Qian, H., 2015b. Integrated modeling of water supply and demand under management options and climate change scenarios in Chifeng City, China. J. Am. Water Resour. Assoc. (JAWRA) 51 (3), 655–671. https://doi.org/10.1111/1752-1688.12311.

Hao, L., Huang, X., Qin, M., Liu, Y., Li, W., Sun, G., 2018. Ecohydrological processes explain urban dry island effects in a wet region, Southern China. Water Resour. Res. 54 (9), 6757–6771.

He, B., Wang, Y., Takase, K., et al., 2009. Estimating land use impacts on regional scale urban water balance and groundwater recharge. Water Resour. Manage. 23, 1863–1873.

Huang, Z., Wang, X., Xiao, Y., Yang, F., Wang, X., 2015. Effect of climate change on rice irrigation requirement in Songnen Plain, Northeast China. J. Appl. Ecol. 26 (1), 260 (In Chinese).

Immerzeel, W.W., Gaur, A., Zwart, S.J., 2008. Integrating remote sensing and a process-based hydrological model to evaluate water use and productivity in a south Indian catchment. Agric. Water Manage. 95, 11–24.

Kang, M., Park, S., Lee, J., Yoo, K., 2006. Applying SWAT for TMDL programs to a small watershed containing rice paddy fields. Agric. Water Manage. 79, 72–92.

Kim, K.H., Cho, J., Yong, H.L., Lee, W.S., 2015. Predicting potential epidemics of rice leaf blast and sheath blight in South Korea under the RCP 4.5 and RCP 8.5 climate change scenarios using a rice disease epidemiology model, EPIRICE. Agric. For. Meteorol. 203, 191–207.

Kim, N.W., Chung, I.M., Won, Y.S., Arnold, J.G., 2008. Development and application of the integrated SWAT–MODFLOW model. J. Hydrol. 356, 1–16.

Kim, Y.-J., Kim, H.-D., Jeon, J.-H., 2014. Characteristics of water budget components in paddy rice field under the asian monsoon climate: application of hspf-paddy model. Water 6, 2041–2055.

Laurent, F., Ruelland, D., 2011. Assessing impacts of alternative land use and agricultural practices on nitrate pollution at the catchment scale. J. Hydrol. 409, 440–450.

Li, C., Sun, G., Cohen, E., Zhang, Y., Xiao, J., McNulty, S.G., Meentemeyer, R.K., 2020. Modeling the impacts of urbanization on watershed gross primary productivity and its tradeoffs with water yield across the conterminous, United States. J. Hydrol.

Lin, B., Chen, X., Yao, H., Chen, Y., Liu, M., Gao, L., James, A., 2015. Analyses of landuse change impacts on catchment runoff using different time indicators based on SWAT model. Ecol. Ind. 58, 55–63.

Liu, Q., Yang, Z., Cui, B., Sun, T., 2010. The temporal trends of reference evapotranspiration and its sensitivity to key meteorological variables in the Yellow River Basin, China. Hydrol. Process. 24, 2171–2181.

Liu, X., Xu, C., Zhong, X., Li, Y., Yuan, X., Cao, J., 2017a. Comparison of 16 models for reference crop evapotranspiration against weighing lysimeter measurement. Agric. Water Manage. 184, 145–155.

Liu, C., Sun, G., McNulty, S.G., Noormets, A., Fang, Y., 2017b. Environmental controls on seasonal ecosystem evapotranspiration/potential evapotranspiration ratio as determined by the global eddy flux measurements. Hydrol. Earth Syst. Sci. 21, 311–322. https://doi.org/10.5194/hess-21-311-2017.

Liu, Y., Youpeng, X.U., Shi, Y., 2012. Hydrological effects of urbanization in the qinhuai river basin, China. Procedia Eng. 28, 767–771.

Locatelli, L., Mark, O., Mikkelsen, P.S., Arnbjerg-Nielsen, K., Deletic, A., Roldin, M.K., Binning, P.J., 2017. Hydrologic impact of urbanization with extensive stormwater infiltration. J. Hydrol. 544, 524–537.

Lu, J.B., Sun, G., McNulty, S.G., Comerford, N.B., 2009. Sensitivity of pine flatwoods hydrology to climate change and forest management in Florida, USA. Wetlands 29

(3), 826–836.
Martin, K.L., Hwang, T., Vose, J.M., Coulston, J.W., Wear, D.N., Miles, B., et al., 2017. Watershed impacts of climate and land use changes depend on magnitude and land use context. Ecohydrology 10.
Mauser, W., Schädlich, S., 1998. Modelling the spatial distribution of evapotranspiration on different scales using remote sensing data. J. Hydrol. 212, 250–267.
Merritt, W.S., Alia, Y., Barton, M., Taylor, B., Cohen, S., Neilsen, D., 2006. Hydrologic response to scenarios of climate change in subwatersheds of the Okanagan basin, British Columbia. J. Hydrol. 326, 79–108.
Miyazaki, N., Kamewada, K., Iwasaki, S., 2005. Quality changes of agricultural water passing through paddy fields. Bull. Tochigi Agric. Exp. Stn. 55, 45–55.
Mcleod, M.K., Daniel, H., Faulkner, R., Murison, R., 2004. Evaluation of an enclosed portable chamber to measure crop and pasture actual evapotranspiration at small scale. Agric. Water Manage. 67, 15–34.
Moriasi, D.N., Arnold, J.G., Van Liew, M.W., Binger, R.L., Harmel, R.D., and Veith, T.L., 2007. Model evaluation guidelines for systematic quantification of accuracy in watershed simulations. Soil Water Div. ASABE, 50.
Nash, J.E., Sutcliffe, J.V., 1970. River flow forecasting through conceptual models: Part1-A discussion of principles. J. Hydrol. 10, 282–290.
Neitsch S.L., Arnold J.G., Kiniry J.R., Williams J.R., King K.W. Soil and Water Assessment Tool Theoretical Documentation Version 2000: TR-191. Texas Water Resources Institute, College Station, TX. 2002.
Nguyen, Q. H., and Kappas, M., 2015. Modeling Surface Runoff and Evapotranspiration using SWAT and BEACH for a Tropical Watershed in North Vietnam, Compared to MODIS Products.
Nie, W., Yuan, Y., Kepner, W., Nash, M.S., Jackson, M., Erickson, C., 2011. Assessing impacts of Landuse and Landcover changes on hydrology for the upper San Pedro watershed. J. Hydrol. 407, 105–114.
Oudin, L., Salavati, B., Furusho-Percot, C., Ribstein, P., Saadi, M., 2018. Hydrological impacts of urbanization at the catchment scale. J. Hydrol. 559, 774–786.
Paul, M.J., Meyer, J.L., 2011. Streams in the urban landscape. Annu. Rev. Ecol. Syst. 32, 333–365.
Paul, S., Cashman, M.A., Szura, K., Pradhanang, S.M., 2017. Assessment of nitrogen inputs into hunt river by onsite wastewater treatment systems via SWAT simulation. Water 9, 610.
Piao, S., Ciais, P., Huang, Y., Shen, Z., Peng, S., Li, J., Zhou, L., Liu, H., Ma, Y., Ding, Y., 2010. The impacts of climate change on water resources and agriculture in China. Nature 467, 43.
Qiu, R., Du, T., Kang, S., Chen, R., Wu, L., 2015. Assessing the simdualkc model for estimating evapotranspiration of hot pepper grown in a solar greenhouse in northwest china. Agric. Syst. 138, 1–9.
Qin, M., Hao, L., Sun, L., Liu, Y., Sun, G., 2019. Climatic controls on watershed reference evapotranspiration varied during 1961–2012 in Southern China. J. Am. Water Resour. Assoc. 55 (1), 189–208.
Sakaguchi, A., Eguchi, S., Kato, T., Kasuya, M., Ono, K., Miyata, A., Tase, N., 2014. Development and evaluation of a paddy module for improving hydrological simulation in SWAT. Agric. Water Manage. 137, 116–122.
Shiri, J., Kişi, Ö., Landeras, G., López, J.J., Nazemi, A.H., Stuyt, L.C., 2012. Daily reference evapotranspiration modeling by using genetic programming approach in the Basque Country (Northern Spain). J. Hydrol. 414, 302–316.
Silva, B., Strobl, S., Beck, E., Nendix, J., 2016. Canopy evapotranspiration, leaf transpiration and water use efficiency of an andrean pasture in SE-Ecuador–a case study. Erdkunde 70, 5–18.
Sun, G., and Lockaby, B. G., 2012. Water quantity and quality at the urban–rural interface, Urban–Rural Interfaces: Linking People and Nature, 29-48.
Sun, L., Yang, L., Hao, L., Fang, D., Jin, K., Huang, X., 2017. Hydrological Effects of vegetation cover degradation and environmental implications in a semiarid temperate steppe, China. Sustainability 9, 281.
Sun, P., Wu, Y., Xiao, J., Hui, J., Hu, J., Zhao, F., et al., 2019. Remote sensing and modeling fusion for investigating the ecosystem water-carbon coupling processes. Sci. Total Environ. 697, 134064.
Tsai, M. H., 2002. The Multi-functional roles of paddy field irrigation in Taiwan. Proceedings of the pre-symposium for the third world water forum (WWF3), pp. 217–220.
Wang, J. Li, F. and Yi, J. The forecasting and regulation hydraulic model of Qinhuai River catchment. Sciencepaper online 2006. http://www.paper.edu.cn. (In Chinese).
Wang, K., Liang, S., 2008. An improved method for estimating global evapotranspiration based on satellite determination of surface net radiation, vegetation index, temperature, and soil moisture. J. Hydrometeorol. 9, 712–727.
Wang, Y.Q., Xiong, Y.J., Qiu, G.Y., Zhang, Q.T., 2016. Is scale really a challenge in evapotranspiration estimation? A multi-scale study in the Heihe oasis using thermal remote sensing and the three-temperature model. Agric. For. Meteorol. 230.
Wang, W., Sun, F., Peng, S., Xu, J., Luo, Y., Jiao, X., 2013. Simulation of response of water requirement for rice irrigation to climate change. Trans. Chin. Soc. Agric. Eng. 29 (14), 90–98 (In Chinese).
Wu, J., Kutzbach, L., Jager, D., Wille, C., Wilmking, M., 2015. Evapotranspiration dynamics in a boreal peatland and its impact on the water and energy balance. J. Geophys. Res. Biogeosci. 115, 4038.
Wu, Y., Liu, S., Qiu, L., Sun, Y., 2016. SWAT-DayCent coupler: an integration tool for simultaneous hydro-biogeochemical modeling using SWAT and DayCent. Environ. Modell. Software 86, 81–90.
Xie, X., Cui, Y., 2011. Development and test of SWAT for modeling hydrological processes in irrigation districts with paddy rice. J. Hydrol. 396, 61–71.
Xu, J., Liu, X., Yang, S., Qi, Z., Wang, Y., 2017. Modeling rice evapotranspiration under water-saving irrigation by calibrating canopy resistance model parameters in the Penman-Monteith equation. Agric. Water Manage. 182, 55–66.
Xu, X., Yang, D., 2010. Analysis of catchment evapotranspiration at different scales using bottom-up and top-down approaches. Front. Archit. Civ. Eng. China 4, 65–77.
Yang, L., Li, C., Wang, S., Yang, W., 2014. Sensitive analysis of potential evapotranspiration to key climatic factors in Taohe River Basin. Trans. Chin. Soc. Agric. Eng. 30, 102–109.
Yang, Y., 2014. A hybrid dual-source model of estimating evapotranspiration over different ecosystems. Remote Sens. 6, 8359–8386.
Zhang, B., Xu, D., Liu, Y., Li, F., Cai, J., Du, L., 2016. Multi-scale evapotranspiration of summer maize and the controlling meteorological factors in north China. Agric. For. Meteorol. 216, 1–12.
Zhang, X., Xu, Y.P., Fu, G., 2014. Uncertainties in SWAT extreme flow simulation under climate change. J. Hydrol. 515, 205–222.
Zhao, F., Wu, Y., Bellie, S., Long, A., Qiu, L., Chen, J., 2019a. Climatic and hydrologic controls on net primary production in a semiarid loess watershed. J. Hydrol.
Zhao, A., Zhu, X., Liu, X., Pan, Y., Zuo, D., 2015. Impacts of land use change and climate variability on green and blue water resources in the Weihe River Basin of northwest China. Catena 137, 318–327.
Zhao, F., Wu, Y., Bellie, S., Long, A., Qiu, L., Chen, J., et al., 2019b. Climatic and hydrologic controls on net primary production in a semiarid loess watershed. J. Hydrol. 568, 803–815.
Zhao, F., Wu, Y., Yao, Y., Sun, K., Zhang, X., Winowiecki, L., et al., 2020a. Predicting the climate change impacts on water-carbon coupling cycles for a loess hilly-gully watershed. J. Hydrol. 581, 124388.
Zhao, F., Wu, Y., Wang, L., Liu, S., Wei, X., Xiao, J., et al., 2020b. Multi-environmental impacts of biofuel production in the U.S. Corn Belt: a coupled hydro-biogeochemical modeling approach. J. Cleaner Prod. 251, 119561.
Zhao, L., Lee, X., R., B., Smith and K., Oleson, 2014. Strong contributions of local background climate to urban heat islands. Nature, 511(7508):216-219.
Zheng, Q.Z., Hao, L., Huang, X.L., Sun, L., Sun, G., 2020. Effects of Urbanization on Watershed Evapotranspiration and Its Components in Southern China. Water 12, 645.
Zhou, F., Xu, Y., Chen, Y., Xu, C.-Y., Gao, Y., Du, J., 2013. Hydrological response to urbanization at different spatio-temporal scales simulated by coupling of CLUE-S and the SWAT model in the Yangtze River Delta region. J. Hydrol. 485, 113–125.
Zhu, C., Li, Y., 2014. Long-term hydrological impacts of land use/land cover change from 1984 to 2010 in the little river watershed. Tennessee Int. Soil Water Conserv. Res. 2, 11–21.